Experimental Thermal and Fluid Science 130 (2022) 110514

Contents lists available at ScienceDirect

Experimental Thermal and Fluid Science

journal homepage: www.elsevier.com/locate/etfs

Effects of chamber pressure on the kinematic characteristics of spray flows exhausted from an airblast atomizer

Zichen Zhang, Yang Liu, Hui Hu *

Department of Aerospace Engineering, Iowa State University, Ames, IA 50011, USA

ARTICLE INFO

Keywords:
Spray characteristics
Kinematic similarity
Airblast atomizer
Chamber pressure effects
Stokes number
Stereoscopic PIV measurements

ABSTRACT

An experimental investigation was conducted to examine the air–liquid interactions in the spray flows exhausted from an airblast atomizer at different ambient pressures. The experimental study was conducted in a specially designed high-pressure spray test rig available at Iowa State University. During the experiments, while the pressure drop ratio across the airblast atomizer was fixed at a pre-selected value, the pressure in the test chamber was increased from 0.10 MPa (i.e., at ~1.0 bar) up to 0.72 MPa (i.e., at 7.2 bar) to simulate the scenario in the combustion chambers of small turboprop engines. A high-resolution stereoscopic particle image velocimetry (SPIV) system was used to measure the velocity fields of the airflow and spray droplets separately. While the airflow characteristics were found to be almost insensitive to the chamber pressure, the kinematic characteristics of the spray droplets were found to change significantly as the chamber pressure increases. A cross-correlation operation was performed to characterize the effects of the chamber pressure on the kinematic similarity of the spray droplets to the airflow. An improved formula was derived to estimate the corresponding Stokes number values of the spray droplets at different chamber pressures. It was revealed clearly that, a higher chamber pressure would lead to greater aerodynamic forces acting on the spray droplets to intensify the air–liquid interactions and promote the breakup of large droplets into finer droplets. As a result, while the average size of spray droplets exhausted from the same airblast atomizer was found to decrease substantially with the increasing chamber pressure, the finer droplets with smaller Stokes number values would follow the local airflow more faithfully, resulting in a higher kinematic similarity between the spray droplets and airflow at higher chamber pressures.

1. Introduction

It is well known that the process of breaking up or atomization of liquid fuel into droplets in the form of a fine spray plays a pivotal role in improving energy efficiency and suppressing pollutant formation while meeting the operability requirements for aero-engines. Significant improvements in aero-engine performances can be achieved by having the ability to control the spray characteristics through optimal design of liquid fuel atomizers. Airblast atomizers, which generate sprays by exhausting slow-moving liquids into high-velocity air streams, are widely used because of the great benefits in improving fuel efficiency, suppressing pollutant formation, and meeting environmental regulations for aero-engines [1]. Unlike conventional liquid fuel atomizers depending solely on the ultra-high injection pressure for the fuel atomization, airblast atomizers would utilize swirling airflows to enhance the air–liquid interactions for more efficient atomization, while the airflow exhaust from airblast atomizers can also be further utilized in the combustion afterward [2].

Extensive studies have been conducted in recent years on the characteristics of the liquid sprays exhausted from airblast atomizers [3–5]. Klein [4] reported that swirling airflow exhausted from airblast atomizers is very efficient to achieve rapid mixing between fuel droplets and airflow, which is essential for desirable combustion efficiency. Rizkalla et al. [5] suggested that a higher air injection pressure to an airblast atomizer would result in a greater airflow velocity, which can improve the spray quality by reducing the mean droplet size. Urban et al. [6] found that preheating viscous fuel (e.g., crude rapeseed oil) is beneficial for obtaining finer sprays exhausted from airblast atomizers. Rizk & Lefebvre [7] suggested that the optimum arrangement of airblast atomizers would be a swirling liquid jet surrounded by a coflowing air stream. Fan et al. [8] also reported that airblast atomizers with such design features can produce finer spray droplets, due to the stronger

* Corresponding author.
E-mail address: huhui@iastate.edu (H. Hu).

https://doi.org/10.1016/j.expthermflusci.2021.110514
Received 25 March 2021; Received in revised form 3 August 2021; Accepted 26 August 2021
Available online 1 September 2021

shear stress induced by the swirling airflow to enhance the air–liquid interactions. Inamura et al. [9] found that the droplet size distribution could become much broader with the increasing thickness of the liquid film accumulated at the prefilmer edges of airblast atomizers. Chaussonnet et al. [10] suggested that, while the mechanisms of liquid breakup and atomization would stay the same under different ambient pressures, the variations of the ambient pressure could affect microscopic characteristics of spray flows exhausted from the airblast atomizer (i.e., liquid breakup length and droplet size) by affecting airflow density and aerodynamic drag forces acting on the spray droplets.

It should be noted that, while airblast atomizers are usually used to inject liquid fuel droplets into combustion chambers of aero-engines at substantially elevated chamber pressures (i.e., up to 2.0 MPa for modern aero-engines [11]), many of previous studies on spray characteristics of airblast atomizers were conducted with the pressure of the test chambers at an atmospheric pressure (i.e., ~0.10 Mpa). Only a limited number of studies can be found in the literature to examine the characteristics of spray flows exhausted from airblast atomizers at elevated chamber pressures. He et al. [12] found that the characteristics of spray flows exhausted from the same airblast atomizers under elevated chamber pressures would be significantly different from those under an atmospheric pressure, due to the effects of the gas density and associated aerodynamic forces. Rizk & Lefebvre [13] and Chrigui et al. [14] reported that the average size of the spray droplets exhausted from the same airblast atomizer was reduced substantially under elevated chamber pressure levels. Fu and Yang [15] found that, for a given pressure drop ratio across an airblast atomizer, the spray angle was found to be decreased substantially as the chamber pressure increases. Furthermore, while the density increase of the airflow under elevated chamber pressures would lead to greater aerodynamic forces acting on spray droplets, the momentum loss of the spray droplets became substantial as the droplets moving downstream. Although those previous studies have uncovered useful information, the effects of the chamber pressure on the air–liquid interactions in the spray flows after exhausted from airblast atomizers have not been well understood [16]. More comprehensive studies are highly desirable to elucidate the underlying physics for a better understanding of the dynamic interactions between the airflow and spray droplets at elevated chamber pressure levels, which is essential to explore/optimize the design paradigm of airblast atomizers for maximized energy efficiency, while minimizing pollutant emissions from aero-engines.

In the present study, a comprehensive investigation was conducted to examine the effects of the chamber pressure on the air–liquid interactions in the spray flows exhausted from an airblast atomizer. The experimental study was conducted by leveraging a specially designed high-pressure spray test rig available at Iowa State University. During the experiments, while the pressure drop ratio across the airblast atomizer was fixed at a pre-selected value to maintain a constant total velocity of the airflow exhausted from the atomizer, the pressure in the test chamber of the high pressure test rig was increased from 0.10 MPa (i.e., at an atmosphere pressure) up to 0.72 MPa to simulate the evaluated chamber pressure environments in the combustor of turboprop engines [17]. A high-resolution stereoscopic particle image velocimetry (SPIV) system was used to achieve whole field measurements of the velocity distributions of the airflow and the spray droplets separately. Based on the SPIV measurement results, a cross-correlation operation was performed to quantify the kinematic similarity between the airflow and the spray droplets at different chamber pressure levels. A theoretical analysis was also conducted to derive an improved formula in estimating the Stokes number of the spray droplets at different chamber pressures to elucidate the underlying physics for a better understanding of the effects of the chamber pressures on the air–liquid interactions in the spray flows.

In the context that follows, the experimental setup used in the present study is described at first for characterizing the air–liquid interactions of spray flows exhausted from an airblast atomizer. Then, the SPIV measurement results are presented to quantify the kinematic characteristics of the airflow and spray droplets under different testing conditions, followed by a cross-correlation operation to quantify the kinematic similarity between the spray droplets and the airflow. A comprehensive theoretical analysis is also presented to elucidate the underlying physics pertinent to the effects of the chamber pressure on the traceability of the droplets to follow the local airflow for a better understanding of air–liquid interactions in the spray flows.

2. Experimental setup

The high-pressure spray test rig used for the present study is shown schematically in Fig. 1, which is featured by a cylindrical testing chamber made of alumina with an inner diameter of 220 mm, a length of 470 mm, and 25.4 mm wall thickness. Three circular-shaped observation windows are installed at the same height of the testing chamber with the angles enclosed by the neighboring windows being 120°. The observation windows have a double-wall design with the inner window walls rotating at the desired rotational speeds (i.e., at ~2,000 rpm) to prevent the spray droplets from sticking onto the walls of the observation windows during the experiments. Three big high-pressure tanks (8.0 m^3 in volume and 1.0 MPa in rated pressure at full capacity) and an air compressor (Ingersoll Rand Nirvana^{TM}) were used to supply high-pressure air for the experimental study. Pressure settings in the liquid and air paths are regulated by a series of pneumatic control valves to adjust the pressure levels of the high-pressure spray test rig. A high-speed data acquisition system is integrated with the high-pressure test rig to monitor the temperature and the pressure inside the test chamber. A ball valve is installed at the exit of the high-pressure test rig to adjust the air pressure in the test chamber and to make sure the pressure drop ratio of the airflow across the airblast atomizer was maintained at a pre-selected value under different test conditions.

Fig. 2 shows the schematics of the airblast atomizer used in the present study, which is sited inside an air-conditioned room at a constant temperature of 20.0 ± 1.0 °C. The airblast atomizer, which has an outer diameter of $d = 25.4$ mm, is consisted of an inner high-swirling air path, an outer low-swirling air path, and a liquid fuel path between the two airflow streams. 10 guide vanes were designed in the liquid path to from swirl slits. While the airflow exhausted from the outer air path occupies 80% of the total mass of the injected air flowrate, the inner air path would inject the rest of the 20% air mass. Further information about the design of the airblast atomizer can be found in Pack et al. [18].

Deionized (DI) water was used as the working liquid for the present study, its dynamic viscosity, surface tension and density are 1.00 mPa·s, 72.86 mN/s and 998.21 kg/m^3, respectively [2]. The temperatures of the air and liquid streams were monitored during the experiments by using high-sensitive thermocouple probes (Type-K, Omega^{TM}). It was found that the measured temperatures of the air and liquid streams remained almost unchanged (i.e., within ±0.5 °C) under different test conditions.

During the experiments, the pressure drop ratio of the air stream across the atomizer was set at a constant value (i.e., at 4.0% of the pre-selected chamber pressure) in order to maintain the same total injection velocity of the airflow exhausted from the airblast atomizer [19]. While the velocity of the airflow was set at a constant value, the mass flowrate of the air stream would increase with the chamber pressure due to the higher air density. Table 1 summarizes the mass flowrates of the air and liquid streams supplied to the airblast atomizer for the different test cases examined in the present study (i.e., at different chamber pressure levels).

A high-resolution, Stereoscopic Particle Image Velocimetry (SPIV) system was used in the present study to measure the velocity fields of the spray droplets and airflow exhausted from the airblast atomizer separately. For the SPIV measurements, a double-pulsed Nd:YAG laser (Quantel EverGreen − 200 mJ) integrated with a set of optical lenses was used to generate a laser sheet with a thickness of 1.0 mm to

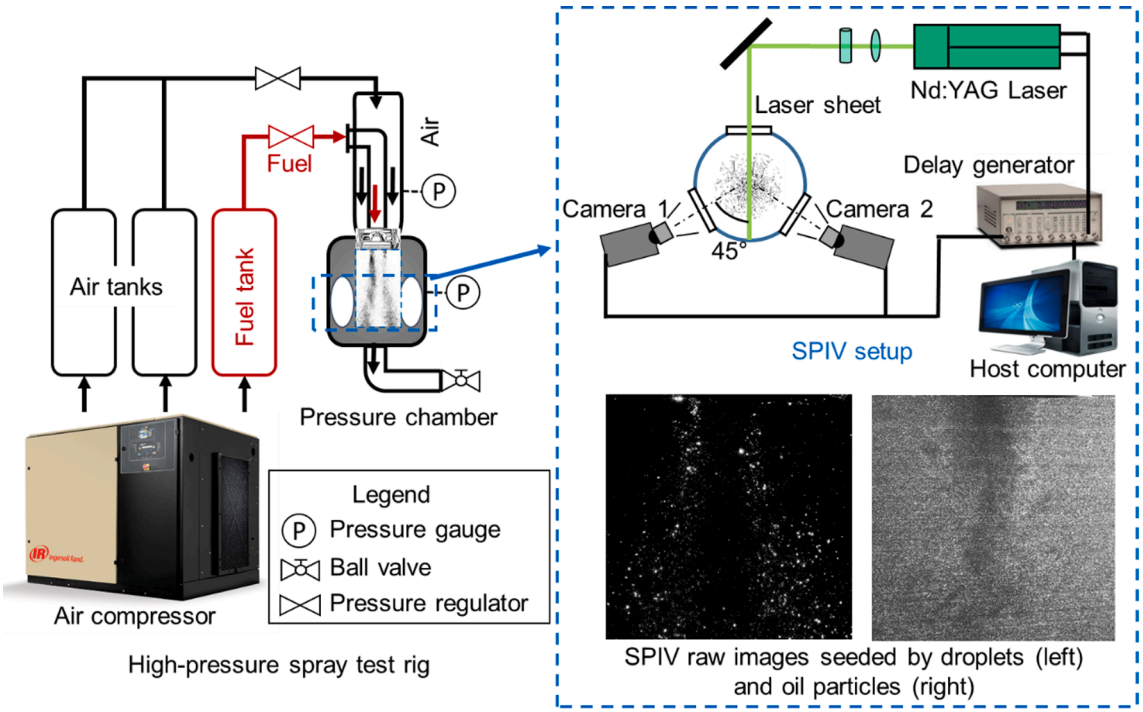

Fig. 1. Schematic of the high-pressure spray test rig used in the present study.

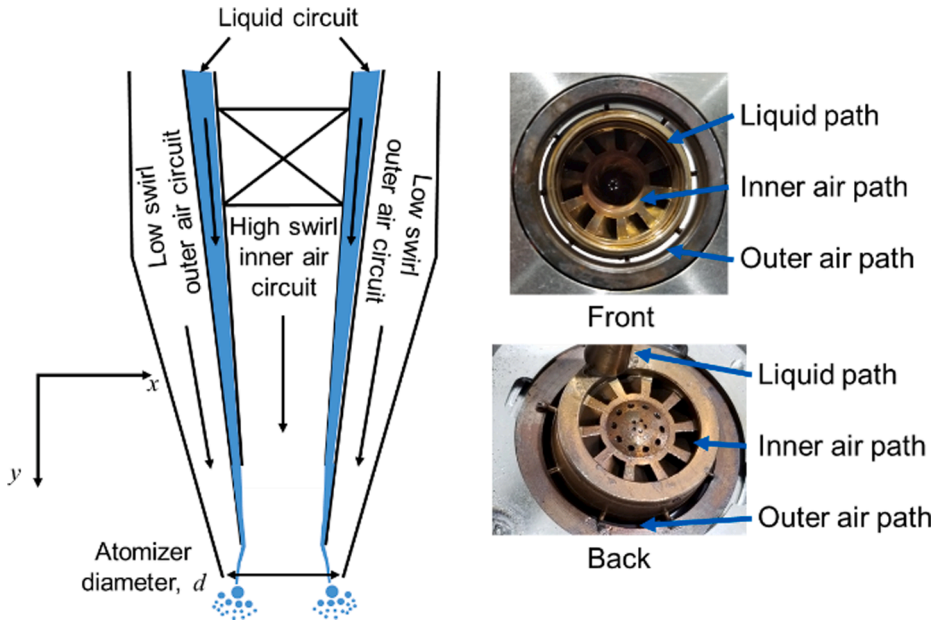

Fig. 2. The airblast atomizer used in the present study.

Table 1
The mass flowrate of air and liquid of different test cases.

Chamber pressure P, (MPa)	0.10	0.24	0.72
Mass flowrate of air, $\dot{m}_{air}$, (g/s)	11.00	23.00	75.00
Mass flowrate of the liquid, $\dot{m}_{liquid}$, (g/s)	0.40	0.40	0.40

illuminate the flow field in the area of interest. The laser sheet was aligned along the center of the airblast atomizer. The images of the tracer particles seeded in the airflow, or the images of the spray droplets were recorded by two high-resolution cameras (PCO-2000 of PCO-Tech^{TM} with the image resolution of 2048 pixels by 2048 pixels). The two cameras were arranged in the forward scattering direction of the laser sheet, and the angle enclosed by the cameras and the illuminating laser sheet was set to be 45°. The two cameras and the Nd: YAG laser were synchronized by using a delay generator (Berkeley Nucleonics, Model 565) working at a sampling frequency of 10 Hz. While A general in-situ calibration procedure was conducted to obtain the mapping functions between the image planes and object planes for the SPIV measurements [20], the acquired PIV images was found to have a spatial resolution of 0.03 mm/pixel. The time interval between the two laser pulses was varied from 2.0 μs to 6.0 μs for different test cases.

Lavision FlowMaster^{TM} software was used to derive all three-components of the velocity vectors from the acquired SPIV images. A frame-to-frame cross-correlation technique was adopted to determine the instantaneous flow velocity vectors from the acquired PIV images with an interrogation window size of 32 pixels × 32 pixels by considering the trading off of the PIV measurement accuracy and spatial resolution[21,22]. An effective overlap of 50% of the interrogation windows was employed in PIV image processing, resulting in a spatial resolution of about 0.50 mm × 0.50 mm for the SPIV measurements.

In the present study, the velocity fields of airflow and spray droplets were measured separately. For the measurements of the airflow velocity, while the liquid path was turned off, a smoke generator was used to generate ~1.0 μm smoke particles as the tracers to seed into the airflow for the SPIV measurements [23]. When the velocity fields of the spray droplets were measured, the injection of the smoke particles into the airflow was stopped, the spray droplets exhausted from the airblast atomizer were used as the tracers for the SPIV measurements. The effects of the liquid injection on the characteristics of the airflow were believed to be negligible since the mass flowrate of the air stream is much greater than that of the liquid stream for the test cases of the present study, as given in Table 1.

It should also be noted that, while the spurious vectors in each frame of the instantaneous SPIV measurements were found to be less than 1.0%, a comprehensive PIV post-processing procedure was used for subpixel interpolations and replacing the spurious velocity vectors with the values from averaging the neighboring vectors. While 1,000 frames of instantaneous SPIV measurements were used to calculate the mean flow quantities for each test cases, the accuracy level of the time-averaged velocity fields for both the airflow and spray flow (i.e., liquid droplets) is expected to be less than 2.0%.

3. Measurement results and discussions

3.1. SPIV measurements to characterize the spray flows in the test chamber

As aforementioned, a high-resolution SPIV system was used to measure the velocity fields of the airflow and spray flow separately in order to examine air–liquid interactions in the spray flows after exhausted from the airblast atomizer under different test conditions. Fig. 3 and Fig. 4 give typical SPIV measurement results in terms of the velocity distributions of the airflow and the spray droplets in the test chamber with chamber pressure changing from $P = 0.1$ MPa to $P = 0.72$ MPa. While the origin of the coordinate is selected at the center of the exit of the airblast atomizer, the coordinates along each axis are normalized by the inner diameter of the atomizer (i.e., $d = 25.4$ mm). The measured velocity fields are normalized by the total velocity of the airflow at the exit of the airblast atomizer (i.e., V_{iso}).

Following up the work of Chen & Yang [19], the total velocity of the airflow is defined as $V_{iso} = \sqrt{2(P_i - P_c)/P_c RT}$, where P_i, P_c, R and T are air injection pressure, chamber pressure, gas constant and chamber temperature, respectively. The term of $(P_i - P_c)/P_c$ is referred as the ratio of pressure difference across the airblast atomizer to the chamber pressure. As described above, the pressure drop ratio was kept at a constant value (i.e., 4.0%) in the present study to minimize the effects of the total velocity of the airflow on the kinematic characteristics of the spray flows exhausted from the airblast atomizer.

For the SPIV measurement results given in Fig. 3 and Fig. 4, while the vector fields illustrate the measured radial velocity component (U) and axial velocity component (V) within the measurement plane, the contour plots show the azimuthal velocity component (W) out of the measurement plane. It can be seen clearly that the velocity fields of the airflow shown in Fig. 3 were found to have a very similar distribution pattern with the normalized velocity magnitude increasing only slightly (i.e., within 10%, probably due to the slight variations in the discharge coefficient of the atomizer at different operating conditions) even though the chamber pressure was increased from 0.10 MPa to 0.72 MPa (i.e., increased by 7.2 times). It indicates that the chamber pressure has only very limited effects on the kinematic characteristics of the airflow exhausted from the airblast atomizer. The very weak dependance of the airflow characteristics on the chamber pressure is believed to be contributed by the constant pressure drop ratio of the airflow during the experiments, since the total velocity of the airflow (V_{iso}) is only a function of the pressure drop ratio, instead of being dependent on the absolute value of the chamber pressure.

However, as shown clearly in Fig. 4, the measured velocity fields of the spray flow (i.e., liquid droplets) under relatively low chamber pressure (i.e., $P = 0.1$ MPa) was found to be very different from those under elevated chamber pressures (i.e., $P = 0.24$ MPa and 0.72 MPa). While the SPIV measurement results given in Fig. 3 reveal that the airflow velocity fields were almost independent of the chamber pressure, the velocity vectors of the spray droplets were found to increase substantially as the chamber pressure increases, especially for the azimuthal components of the droplet flying velocity, as shown clearly in Fig. 4. One of the reasons why the velocities of the spray droplets were found to become much higher at the elevated chamber pressure levels is believed to be closely related to the fact that, the higher air density caused by the greater chamber pressure would result in larger aerodynamic forces acting on the spray droplets [12]. Therefore, the spray droplets could be accelerated much faster for the test cases with higher chamber pressures, in comparison to those droplets at lower chamber pressures. In addition to the magnitude changes in the flying velocities of the spray droplets, the distribution pattern of the spray droplets at the lower chamber pressure (i.e., $P = 0.10$ MPa) was also found to be much different from those under the elevated chamber pressure levels (i.e., $P = 0.24$ MPa and 0.72 MPa). In comparison to the test cases with higher chamber pressures, the spray droplets at lower chamber pressures were found to have greater radial velocity components.

Based on the significant differences in the flying velocities of the droplets within the spray flows from those in the surrounding regions as

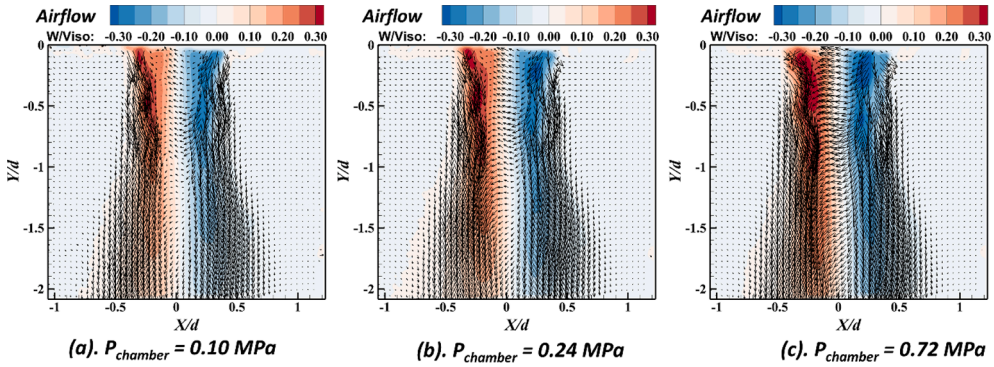

Fig. 3. Time-averaged SPIV measurement results of the airflow in the test chamber.

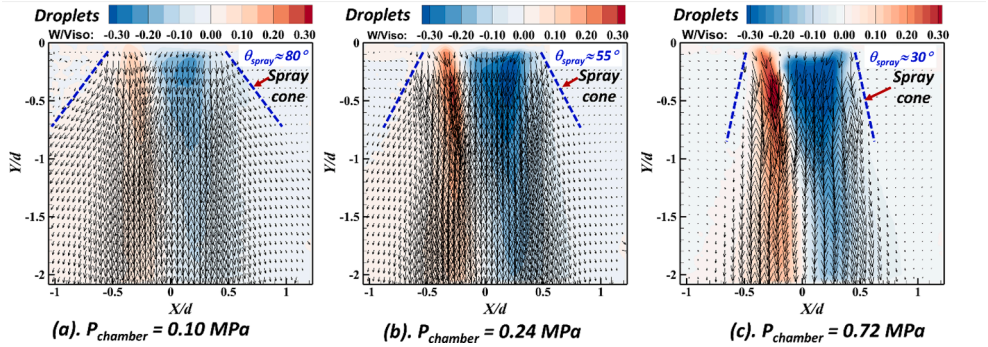

Fig. 4. Time-averaged SPIV measurement results of the spray droplets in the test chamber.

revealed clearly from the SPIV measurement results, the outer boundaries of the spray flows can be easily identified, which are shown as the blue dash lines in Fig. 4. As a result, the cone angles of the spray flows (i.e., the angle between the dash lines) under different chamber pressures can be determined subsequently based on the SPIV measurements. It was revealed clearly that, the cone angle of the spray flow exhausted from the same airblast atomizer was found to decrease substantially as the chamber pressure increases. More specifically, while the spray cone angle was found to be about 80 deg. (i.e., $\theta_{spray} \approx 80^{\circ}$) at the low chamber pressure of the $P = 0.10$ MPa, the corresponding values were

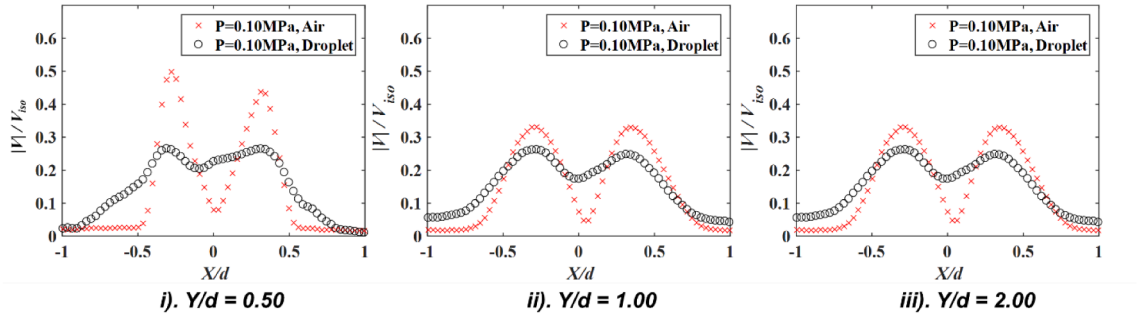

(a). At the chamber pressure of $P = 0.10$MPa

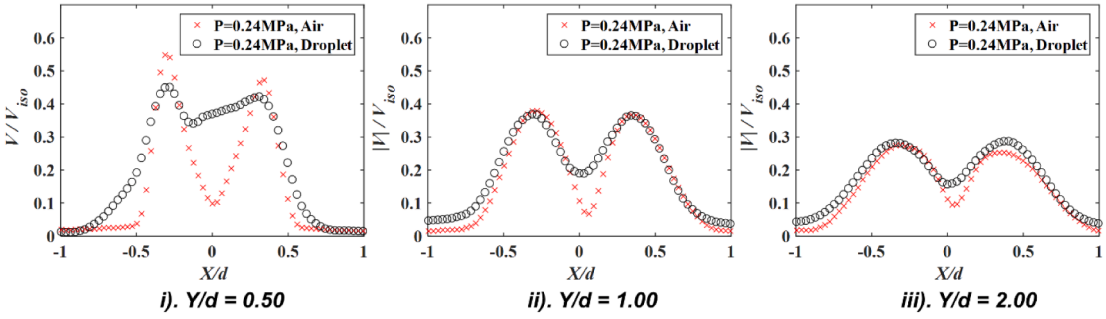

(b). At the chamber pressure of $P = 0.24$MPa

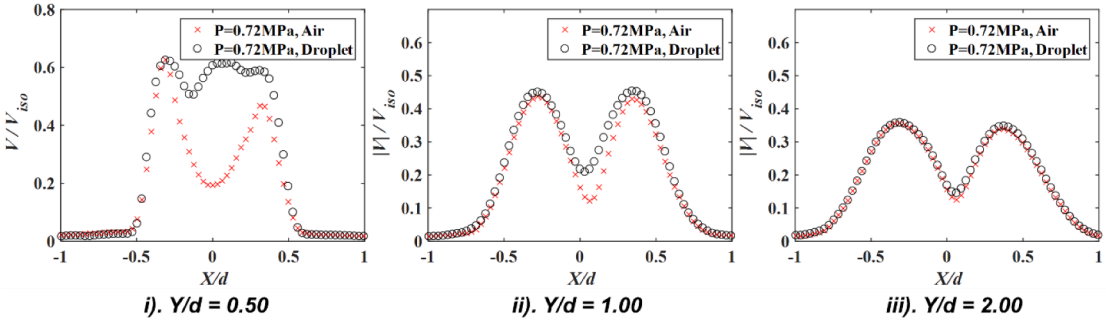

(c). At the chamber pressure of $P = 0.72$MPa.

Fig. 5. Transverse velocity profiles of the airflow and spray droplets at three typical downstream locations at different chamber pressures.

found to become only 55 deg. and 30 deg. (i.e., $\theta_{spray} \approx 55^{\circ}$ and 30°) at the elevated chamber pressure of $P = 0.24$ MPa and 0.72 MPa, respectively. Such a feature revealed from the present SPIV measurements confirmed again that many previous spray experiments conducted with a relatively low chamber pressure (i.e., $P = 0.10$ MPa) would significantly overestimate the spray cone angle in simulating the real scenario taking place inside the combustion chambers of aero-engines with much higher chamber pressures. It should be noted that, even though the experimental observation was reported in a number of previous studies [24–26], very little can be found in the literature to provide clear explanations on why the measurements conducted with low chamber pressures would overestimate the spray cone angles. With this in mind, we conducted the present study is to elucidate the underlying physics pertinent to the experimental observation of the decreasing spray cone angle with the increasing ambient pressures.

Based on the SPIV measurement results given in Fig. 3 and Fig. 4, transverse velocity profiles of the airflow and spray droplets were extracted at three typical downstream locations, i.e., $Y/d = 0.5$, 1.0, and 2.0, respectively. Fig. 5 shows the extracted velocity profiles for both the airflow and the spray flow in the term of normalized velocity magnitudes (i.e., $|V|/V_{iso} = \sqrt{U^2 + V^2 + W^2}/V_{iso}$), which can be used to reveal the effects of the chamber pressure on the characteristics of air–liquid interactions in the spray flows more clearly and quantitatively. As shown quantitatively in Fig. 5(a), for the test case with the chamber pressure being at one atmospheric pressure (i.e., $P = 0.10$ MPa), the peak velocities of the spray flow (i.e., the droplets) were found to be substantially smaller than those of the airflow, especially in the region near the exit of the airblast atomizer (i.e., at the downstream location of $X/d = 0.50$). More specifically, while the normalized peak velocity of the airflow was found to be 0.52, the corresponding value for the spray droplets was found to be only 0.28 at the same downstream location of $Y/d = 0.50$. The regions with relatively high velocity of the spray droplets were found to be much wider than those of the airflow, and the velocities of the spray droplets became even higher than those of the local airflow in the outer periphery of the spray cone. This can be explained by the fact that, due to the swirling motion generated by the airblast atomizer, some of the spray droplets would be more readily to fly radially after exhausted from the airblast atomizer, i.e., moving away from the core region of the spray flow associated with the greater centrifugal forces acting on the droplets, in comparison to the air molecules. As they moving to further downstream locations, the velocity differences between the spray flow (i.e., the droplets) and the airflow were found to become smaller and smaller, due to the intensive air–liquid interactions. At the downstream locations of $Y/d = 2.0$, while the normalized peak velocity of the airflow was found to reduce to ~0.32, the corresponding value for the spray flow droplets was still ~0.28 at the same downstream location for the test case with low chamber pressure (i.e., $P = 0.10$ MPa).

It can also be seen that that, while the variations of airflow characteristics were found to be minimal under different test conditions, the velocities of the spray droplets were found to increase greatly as the chamber pressure increases. For example, at the same downstream location of $Y/d = 0.50$, the maximum value of the normalized velocities of the droplets was found to increase from 0.28 to 0.60 as the chamber pressure was increased from 0.10 MPa to 0.72 MPa. It can also be seen that the differences (i.e., in the terms of both velocity magnitude and distribution patterns) between the velocities of the spray droplets and the airflow were found to become smaller and smaller, as the chamber pressure increases. While the velocity profile of the spray droplets was found to become almost identical as that of the airflow at the downstream location of $Y/d = 2.0$ under the elevated chamber pressure of $P = 0.72$ MPa, there are still significant differences between the velocities of the spray droplets and the local airflow velocities at $Y/d = 2.0$ when the chamber pressure being at one atmospheric pressure (i.e., $P = 0.10$ MPa). It confirms again that the droplets would be more readily to follow the motion of the local airflow under the elevated chamber pressures. It also suggests that the airflow and the spray droplets are becoming more and more kinematically similar as the chamber pressure increases. Such experimental observations are believed to be closely related to the fact that, as the chamber pressure increases, the air density inside the chamber would increase greatly, which would result in much stronger aerodynamic forces acting on the airborne droplets in the test chamber [27]. Therefore, with the much stronger aerodynamic forces acting on the droplets, they would follow the local airflow more faithfully at higher chamber pressures, in comparison to the cases with lower chamber pressures.

It should also be noted that, while an obvious asymmetry feature can be observed in the region near the atomizer exit (i.e., at $Y/d = 0.50$) from the measured droplet velocity profiles given in Fig. 5, the asymmetry feature was found to become much less obvious as the droplets moving to further downstream locations (i.e., at $Y/d = 1.00$ and 2.00). Similar asymmetry feature in the spray flows near atomizer exits can also be can also observed from the measurement results reported in previous studies [28]. This can be explained by the fact that, as revealed clearly in Fig. 2, since guide vanes were arranged with tilted orientation angles in order to form swirl slits for the liquid stream, the tilted guide vanes in the liquid path would cause non-uniform liquid films/ligaments over the prefilmer of the atomizer. It would lead to non-uniform breakups of the liquid films/ligaments into relatively large droplets at the exit of the atomizer [10]. Since the droplets in the region near the atomizer exit are relatively large, their flying trajectories would be affected mainly by the inertia forces which are closely related to the design of the swirling liquid slots inside the atomizer. As a result, the spray flow was found to have an asymmetry feature near the exit of the airblast atomizer. Due to the intensive interactions between the droplets and the swirling airflow in the test chamber, the large droplets would experience a secondary breakup process to form much more finer droplets as they moving downstream [10]. Since the motion of the smaller droplets would be influenced significantly by the surrounding airflow, the asymmetric feature of the spray flow was found to be almost diminished at further downstream locations (i.e., the velocity profiles of the spray flow becoming almost symmetric at $Y/d = 1.00$ and 2.00), as revealed from the SPIV results given in Fig. 5.

3.2. To quantify the kinematic similarity of the spray flow to the airflow under different test conditions via a cross-correlation operation

As revealed clearly from the SPIV measurement results given above, the velocity fields of the spray flow (i.e., liquid droplets) were found to become more and more resembling to those of the airflow in terms of both the velocity magnitude and distribution pattern as the chamber pressure increases. In the present study, a cross-correlation operation is performed in order to quantify the kinematic similarity of the spray flow to the airflow under different test conditions.

Following up the work of Butcher & Spencer [29], the cross-correlation coefficient, R, is calculated based on following equation:

$$R = \left| \frac{\langle U_{droplet} U_{air} + V_{droplet} V_{air} + W_{droplet} W_{air} \rangle}{\sqrt{\langle U^2 + V^2 + W^2 \rangle_{droplet}} \sqrt{\langle U^2 + V^2 + W^2 \rangle_{air}}} \right| \quad (1)$$

where U, V and W denote the measured three velocity components along the radial, axial, and azimuthal directions, respectively. It is apparently that the value of R would be in the range of 0.0 and 1.0, with $R = 1.0$ indicating a perfect kinematic similarity (i.e., the two compared fields are identical), and $R = 0.0$ indicating no similarity (i.e., the compared fields are irrelevant).

Fig. 6 shows the variations of the calculated R-value as a function of the downstream distance away from the exit of the atomizer. It can be seen clearly that, the value of R would increase gradually with the increasing distance away from the atomizer exit, indicating that the velocity distributions of the airflow and spray flow would become more

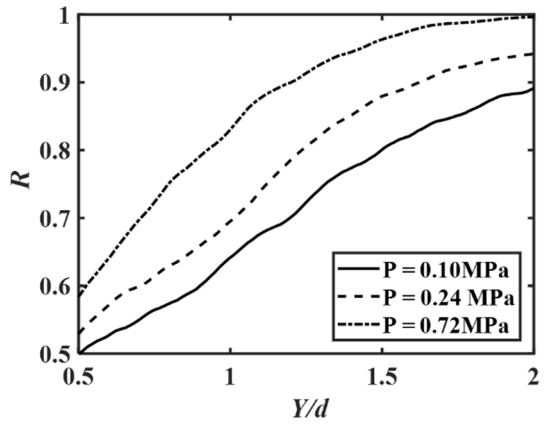

Fig. 6. Variations of the cross-correlation coefficient (R) at different chamber pressure levels.

and more closely coupled at further downstream locations. The increase of the R-value also suggests that spray droplets would follow the local airflow much more closely at the further downstream locations. It can also be seen that, at the same downstream locations, the values of R were found to increase significantly as the chamber pressure increases. A notable example is that the value of R rises from 0.9 to 1.0 at the same downstream location $Y/d = 2.0$ as the chamber pressure increases from $P = 0.10$ MPa to $P = 0.72$ MPa. This can also be explained by that, the greater air density at higher chamber pressure levels would lead to stronger aerodynamic forces acting on the spray droplets, which would intensify the air–liquid interactions to enable the droplets to follow the airflow more faithfully, i.e., better traceability of the droplets under at higher chamber pressures.

3.3. A theoretical analysis to examine the effects of the chamber pressure on the traceability of the spray droplets to follow the local airflow

A comprehensive theoretical analysis was also performed to examine the effects of chamber pressure on the traceability of the spray droplets in order to elucidate the underlying physics for a better understanding about the air–liquid interactions in the spray flows. It is well known that the traceability of an airborne droplet in relation to the surrounding airflow could be characterized by using a non-dimensional parameter [30], named as Stokes number (St), which is defined as the ratio of the relaxation time of the droplet to the characteristic time of the surrounding airflow[28,31], which is usually expressed as:

$$St = \frac{t_0|V|}{d} = \frac{\rho_p d_p^2 |V|}{18\mu d} \tag{2}$$

where t_0, d, ρ_p, d_p and μ are the relaxation time of droplets, the exit diameter of the airblast atomizer, droplet density, droplet size and air viscosity, respectively. When St value is small (i.e., less than one), the airborne droplet would follow the airflow faithfully. If the St value is large (i.e., much greater than one), the droplet would detach from the airflow, especially for the scenario with the airflow having an abrupt acceleration or deceleration [32]. With the classical formula of Eq. (2) to calculate the Stokes number of an airborne droplet, the traceability of an airborne droplet seems to be affected only by the flying velocity and droplet size [33].

It should be noted that the classic formula given in Eq. (2) is only applicable for the scenario with the corresponding Reynolds (Re) number of the airborne droplet is very small (i.e., much less than one) or in Stokes flows. However, the corresponding Re number for the spray droplets of the present study is much greater than one. For example, for a tiny droplet with the diameter of ~20 μm with a nominal flying velocity of 30 m/s (i.e., the typical flying velocity of the spray droplets in the present study), the corresponding Re value would be over 40. Therefore, instead of using the classical formula of Eq. (2), an improved formula is derived in the present study to estimate the Stokes number (St) of the spray droplets with much greater Reynolds number values.

Since the Stokes number (St) is defined as the ratio of the relaxation time of an airborne droplet to the characteristic time of the surrounding airflow [27,31], the key point in deriving a new formula to estimate the Stokes number values of the spray droplets with much greater Re numbers (i.e., much greater than one) is to determine the relaxation time of the spray droplets properly. Information about the aerodynamic forces acting on the spray droplets are needed to determine the relaxation time of the droplets. As described in Goossens [34], the drag coefficient of a droplet with the Re number less than 500 can be approximated by using an empirical equation:

$$C_d = \frac{24}{\mathrm{Re}}\left(1 + 0.15\mathrm{Re}^{0.687}\right) \tag{3}$$

Following up the work of Crowe et al. [32], the characteristic velocity in Eqn. (3) should be the velocity difference between the droplet and airflow (i.e., $|\Delta V|$) in calculating the aerodynamic force exerted by the airflow on the airborne droplet. Therefore, the aerodynamic force acting on the droplet can be estimated as:

$$F_{drag} = 3\pi\mu|\Delta V|d_p\left(1 + 0.15\left(\frac{\rho_g d_p|\Delta V|}{\mu}\right)^{0.687}\right) \tag{4}$$

where ρ_g and μ refer to the density and viscosity of airflow, respectively.

Based on Eqn. (4), it is evident that a greater air density at an elevated ambient pressure would lead to a greater aerodynamic force acting on the spray droplet, which would result in a faster acceleration of the droplet (i.e., reduction of the droplet relaxation time). The acceleration for an airborne droplet can be estimated as:

$$a = \frac{d|\Delta V|}{dt} = \frac{18\mu|\Delta V|}{\rho_p d_p^2}\left(1 + 0.15\left(\frac{\rho_p d_p|\Delta V|}{\mu}\right)^{0.687}\right) \tag{5}$$

Rearranging Eq. (5), it can be expressed as:

$$\frac{\rho_p d_p^2}{18\mu|\Delta V|\left(1 + 0.15\left(\frac{\rho_p d_p|\Delta V|}{\mu}\right)^{0.687}\right)} d|\Delta V| = dt \tag{6}$$

As described in Crowe et al. [32], since the relaxation time of an airborne droplet is referred to be the time needed to accelerate the droplet from zero velocity to the 63% of the airflow velocity (i.e., $(e-1)/e$, where e is Euler's number), the relaxation time of the droplet can be obtained by integrating the term of $|\Delta V|$ from $|V|$ (i.e., airflow velocity) to the value of $|V|/e$. As a result, the relaxation time of the droplet can be expressed as:

$$t_0 = \frac{\rho_p d_p^2}{18\mu}\left(1 - 1.46ln\left(\frac{1 + 0.15\left(\frac{\rho_p d_p|V|}{\mu}\right)^{0.687}}{1 + 0.15\left(\frac{\rho_p d_p|V|}{\mu e}\right)^{0.687}}\right)\right) \tag{7}$$

Substituting Eq. (7) into Eq. (2), the improved formula to quantify the Stokes number of the airborne droplet with its Reynolds number less than 500 is given as:

$$St = \frac{\rho_p d_p^2|V|}{18\mu d}\left(1 - 1.46ln\left(\frac{1 + 0.15Re^{0.687}}{1 + 0.15(Re/e)^{0.687}}\right)\right) \tag{8}$$

It should be noted that, Eq. (8) can be used to evaluate St of spray droplets in a much wider range of Re., in comparison to the classic formula given in Eq. (2). If the Re number is very small (i.e., less than one), Eq. (8) will approach the value given by the classic formula of Eq. (2).

As shown clearly in Eq. (8), in addition to the droplet diameter and

airflow velocity, the value of *St* for an airborne droplet (i.e., the traceability of the droplet to follow the local airflow) would also be affected by the air density. Since the air density is proportional to the chamber pressure, the changes in the chamber pressure would lead to the variations of the Stokes numbers of the airborne droplets, thereby, affecting the traceability of the droplets to follow the local airflow.

Fig. 7 give the estimated *St* values of the spray droplets as a function of the droplet size with a nominal flying velocity of 30 m/s at different chamber pressure levels relevant to the test cases of the present study, which can be used to elucidate the underlying physics for a better understanding on the effects of the chamber pressure on the traceability of the spray droplets to follow the local airflow. It can be seen clearly that, with a fixed droplet diameter, the *St* value of the droplets would decrease substantially as the chamber pressure increases. More specifically, for a spray droplet of ~100 μm in size with a flying velocity of 30 m/s, while the *St* value is estimated to be 8.9 at one atmospheric pressure (i.e., $P = 0.10$ MPa), the corresponding *St* value was found to become only 2.6 under the elevated chamber pressure of $P = 0.72$ MPa. It indicates again that, even for the same size of the spray droplets in the test chamber, the droplets would be more readily to follow the motion of the local airflow at the elevated chamber pressures, resulting in the better kinematic similarity between the spray flow and airflow, as revealed quantitatively from the SPIV measurement results described above.

As revealed clearly in Fig. 7, in addition to the chamber pressure, the *St* value would also be a strong dependent of the droplet size, i.e., the estimated *St* value was found to increase monotonically as the droplet size increases, which agrees with findings reported by Jedelsky et al. [28]. It should be noted that, several previous studies had reported that the average sizes of the spray droplets exhausted from the same airblast atomizer would decrease substantially as the chamber pressure increases [2,6,35]. This can be explained by the fact that, a higher chamber pressure would cause a greater air density in the test chamber and lead to stronger aerodynamic forces acting on the spray droplets, thereby, promoting the secondary breakup of larger droplets into finer droplets due to the stronger air–liquid interactions [26]. Fig. 8 shows the typical acquired raw images of the spray droplets as the chamber pressure was increased from $P = 0.10$ MPa to $P = 0.72$ MPa. While it is very difficult to accurately determine the size of the spray droplets from the acquired images due to the complicated implications of the strong scattering and light refraction on the spray droplets [36], the acquired images can still be used to qualitatively reveal the noticeable size changes of the droplets as the chamber pressure changes. It can be seen clearly that, as the chamber pressure increases from $P = 0.10$ MPa to $P = 0.72$ MPa, the size of the spray droplets was found to decrease substantially, which confirms the research findings reported in the previous studies [2,6,35].

It should also be noted that several empirical formulas/models have been suggested to estimate of the average droplet size of the spray flows after exhausted from airblast atomizers. As described in Tareq et al. [2] and Rizkalla & Lefebvre [5], the average size of the droplets exhausted from an airblast atomizer similar as the one used in the present study can be estimated by using following equation:

$$\frac{SMD}{L_C} = A\left(\frac{\sigma_L}{\rho_g |V|_{air}^2 d_p}\right)^{0.5}\left(1+\frac{\dot{m}_{liquid}}{\dot{m}_{air}}\right) + B\left(\frac{\mu_L^2}{\sigma_L \rho_p d_p}\right)^{0.5}\left(1+\frac{\dot{m}_{liquid}}{\dot{m}_{air}}\right) \quad (9)$$

where SMD, L_c, $\dot{m}_{liquid}$, $\dot{m}_{air}$ and σ_L are the Sauter mean diameter of the droplets, initial liquid film thickness, the mass flowrate of liquid, the mass flowrate of the air, and the liquid surface tension, respectively. Sauter mean diameter (SMD), defined as the ratio of total droplet volume to the total surface area of droplets, is widely used to represent the average size of droplets [9]. *A* and *B* are the constants to be determined empirically based on the atomizer design.

As described in Rizkalla & Lefebvre [5], Eq. (9) has been widely used to estimate the size of spray droplets exhausted from airblast atomizers with reasonably good accuracy over a wide range of experimental conditions, especially for the cases with low-viscosity liquids like the DI water used in the present study. Since the airblast atomizer used in the present study has a very similar design as the one used by Tareq *et al.* [2], the empirical values of L_c, *A* and *B* suggested by *Tareq et al.* [2] (i.e., $A = 1.299$, $B = 34.184$ and $L_c = 0.055$ mm) were adopted in the present study for a rough estimation of the SMD value of the spray droplets exhausted from the airblast atomizer of the present study. Table 2 summarizes the estimated SMD values based on Eq. (9) under the testing conditions examined in the present study.

Based on the data given in Table 2, it can be seen clearly that the SMD of the spray droplets would decrease greatly with the increasing chamber pressure (i.e., SMD value was found to reduce from ~50 μm at the atmospheric pressure of $P = 0.1$ MPa to only ~26 μm at the evaluated chamber pressure of $P = 0.72$ MPa). As a result, the corresponding *St* values were found to decrease much faster, i.e., from 3.3 to only 0.4 accordingly. The much smaller *St* value of the spray droplets at the elevated chamber pressures (i.e., *St* is only *0.4* at the evaluated chamber pressure of $P = 0.72$ MPa) indicates that the spray droplets would be more readily to follow the motion of the local airflow. As a result, the spray flow and the airflow were found to have a better kinematic similarity as the chamber pressure increases.

In summary, the measurement results of the present experimental study reveal clearly that the chamber pressure would play an important role in promoting the air–liquid interactions in the spray flows. With the fixed total velocity of the airflow, a higher chamber pressure would induce a greater air density, leading to larger aerodynamic forces acting on the airborne droplets to intensify the air–liquid interactions. As a result, the corresponding Stokes numbers of the spray droplets were found to decrease rapidly as the chamber pressure increases, enabling the spray droplets to follow the motion of local airflow more faithfully. Furthermore, the higher chamber pressure would also result in smaller size of the spray droplets, which would also lead to better traceability of the spray droplets to the local airflow. Therefore, the spray flow and the airflow were found to have a higher kinematic similarity at higher chamber pressures, as revealed quantitatively from the SPIV measurement results.

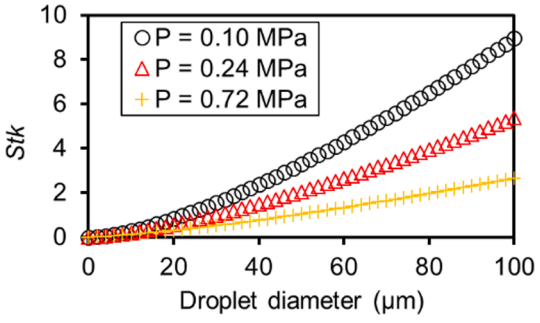

Fig. 7. Variations of the Stokes number (*St*) as a function of the droplet size with a nominal flying velocity of 30 m/s at different chamber pressure levels.

4. Summary and conclusions

A comprehensive investigation was conducted to examine the effects of the chamber pressure on the air–liquid interactions in the spray flows exhausted from an airblast atomizer. During the experiments, while the total velocity of the airflow was fixed at a pre-selected value, the chamber pressure of the high-pressure spray test rig was increased from 0.10 MPa (i.e., at an atmosphere pressure) up to 0.72 MPa (i.e., at ~7.2 times of the standard atmosphere pressure) to simulate the working environments in the combustor chamber of a small aero-engine. A high-resolution stereoscopic particle image velocimetry (SPIV) system was

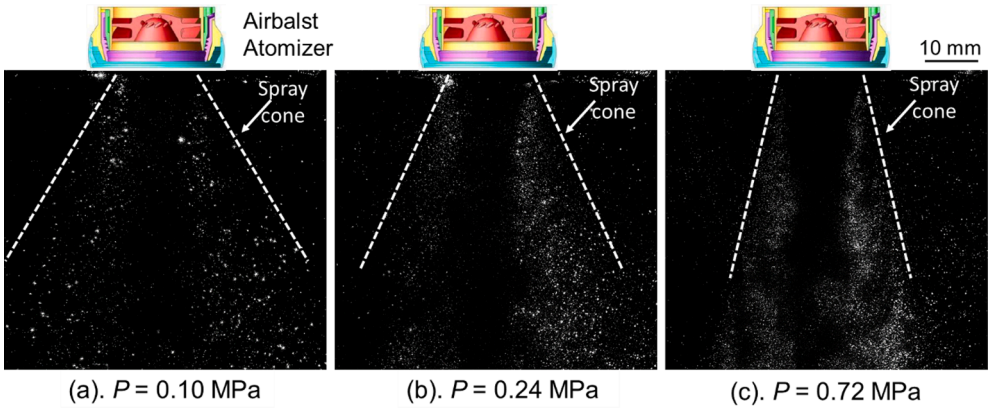

Fig. 8. The acquired images of the spray droplets at different chamber pressures.

Table 2
The estimated Sauter mean diameter (SMD) and corresponding Stokes number (*St*) of the spray droplets under the test conditions examined in the present study.

Chamber pressure level, *P* (MPa)	0.10	0.24	0.72
SMD (μm)	50	36	26
St	3.3	1.3	0.4

used to quantify the velocity fields of the airflow and the spray droplets separately under different test conditions.

After being exhausted from the airblast atomizer, while the characteristics of the airflow were found to be almost independent of the chamber pressure, the velocities of the spray droplets were found to vary significantly as the chamber pressure increases. As the chamber pressure increases, while the velocity magnitudes of the droplets were found to increase substantially, the spray cone angle was observed to decrease monotonically. The SPIV measurements confirm quantitatively that the experimental measurements conducted at an atmospheric pressure condition would greatly overestimate the cone angles of the spray flows in simulating the real scenario taking place inside the combustion chambers of aeroengines at elevated chamber pressures. A cross-correlation procedure was performed to quantify the kinematic similarity between the spray droplets and airflow at different chamber pressure levels, and the kinematic characteristics of spray droplets were found to become more and more similar to those of the airflow as the chamber pressure increases.

An improved formula was derived to estimate the Stokes number of the spray droplets to help shed light on the effects of the chamber pressure on the air–liquid interactions in the spray flows. In addition, an empirical model was used to estimate the average size of the spray droplets exhausted from the airblast atomizer at different chamber pressures. It was revealed clearly that, a higher chamber pressure would lead to greater aerodynamic forces acting on the spray droplets to intensify the air–liquid interactions to promote the breakup of large droplets into finer droplets. As a result, while the average size of spray droplets exhausted from the same airblast atomizer was found to decrease substantially with the increasing chamber pressure, the finer droplets with smaller Stokes number would follow the local airflow more faithfully, resulting in the higher kinematic similarity between the spray droplets and airflow at higher chamber pressures.

It should be noted that, while the present study focuses on elucidating the underlying physics pertinent to the effects of the ambient pressure levels on the kinematic characteristics of the spray flows exhausted from the airblast atomizer, the effects of liquid properties (e.g., liquid viscosity, surface tension and viscoelasticity) or/and ambient temperature on the characteristics of the spray droplets are beyond the scope of the present study. A following-up study will be conducted in the near future to evaluate the effects of the liquid properties by comparing the measurement results of different working fluids (e.g., water against aviation fuel or substitutes such as Jet A-or kerosene). Meanwhile, by integrate a heating system to the high-pressure test rig used in the presents study, the effects of the ambient temperature on the kinematic characteristics of spray droplets and their evaporation process will also be explored in the near future.

CRediT authorship contribution statement

Zichen Zhang: Data curation, Formal analysis,Investigation, Visualization, Writing – original draft. **Yang Liu:** Data curation, Formal analysis, Investigation, Supervision. **Hui Hu:** Conceptualization, Methodology, Formal analysis, Writing – review & editing, Funding acquisition, Project administration, Resources, Supervision.

Declaration of Competing Interest

The authors declare that they have no known competing financial interests or personal relationships that could have appeared to influence the work reported in this paper.

Acknowledgments

The research work is supported partially by “Regents Innovation Fund” Program of the State of Iowa and Collins Aerospace Engine Component Division. The authors would like to thank Mr. Brandon Williams of Collins Aerospace System for the help in setting up the high-pressure test rig used for the present experimental study.

References

[1] R. Ma, B. Dong, Z. Yu, T. Zhang, Y. Wang, W. Li, An experimental study on the spray characteristics of the air-blast atomizer, Appl. Therm. Eng. 88 (2015) 149–156, https://doi.org/10.1016/j.applthermaleng.2014.11.068.
[2] M.M. Tareq, R.A. Dafsari, S. Jung, J. Lee, Effect of the physical properties of liquid and alr on the spray characteristics of a pre-filming airblast nozzle, Int. J. Multiph. Flow. 126 (2020) 103240, https://doi.org/10.1016/j.ijmultiphaseflow.2020.103240.
[3] Q.P. Zheng, A.K. Jasuja, A.H. Lefebvre, Structure of airblast sprays under high ambient pressure conditions, J. Eng. Gas Turbines Power. 3 (1996), https://doi.org/10.1115/96-GT-131.
[4] A. Klein, Characteristics of combustor diffusers, Prog. Aerosp. Sci. 31 (1995) 171–271, https://doi.org/10.1016/0376-0421(95)00006-K.
[5] A.A. Rizkalla, A.H. Lefebvre, The influence of air and liquid properties on airblast atomization, J. Fluids Eng. 97 (1975) 316–320, https://doi.org/10.1115/1.3447309.
[6] A. Urbán, M. Malý, V. Józsa, J. Jedelský, Effect of liquid preheating on high-velocity airblast atomization: from water to crude rapeseed oil, Exp. Therm. Fluid Sci. 102 (2019) 137–151, https://doi.org/10.1016/j.expthermflusci.2018.11.006.
[7] N.K. Rizk, A.H. Lefebvre, Influence of atomizer design features on mean drop size, AIAA J. 21 (1983) 1139–1142, https://doi.org/10.2514/3.8217.

[8] X. Fan, C. Liu, Y. Mu, K. Wang, Y. Wang, G. Xu, Experimental investigations of flow field and atomization field characteristics of pre-filming air-blast atomizers, Energies. 12 (2019), https://doi.org/10.3390/en12142800.
[9] T. Inamura, N. Katagata, H. Nishikawa, T. Okabe, K. Fumoto, Effects of prefilmer edge thickness on spray characteristics in prefilming airblast atomization, Int. J. Multiph. Flow. 121 (2019) 103117, https://doi.org/10.1016/j.ijmultiphaseflow.2019.103117.
[10] G. Chaussonnet, S. Gepperth, S. Holz, R. Koch, H.J. Bauer, Influence of the ambient pressure on the liquid accumulation and on the primary spray in prefilming airblast atomization, Int. J. Multiph. Flow. 125 (2020) 103229, https://doi.org/10.1016/j.ijmultiphaseflow.2020.103229.
[11] Y. Cheng, T. Jin, K. Luo, Z. Li, H. Wang, J. Fan, Large eddy simulations of spray combustion instability in an aero-engine combustor at elevated temperature and pressure, Aerosp. Sci. Technol. 108 (2021) 106329, https://doi.org/10.1016/j.ast.2020.106329.
[12] X. He, C. Chen, Y. Yang, Z. Yan, Experimental study on the flow field distribution characteristics of an open-end swirl injector under ambient pressure, Aerosp. Sci. Technol. 98 (2020) 105691, https://doi.org/10.1016/j.ast.2020.105691.
[13] N.K. Rizk, A.H. Lefebvre, Spray characteristics of plain-jet airblast atomizers, vol. 106, 1983, pp. 634–638. https://doi.org/10.1115/83-gt-138.
[14] M. Chrigui, I.V. Roisman, F.Z. Batarseh, A. Sadiki, C. Tropea, Spray generated by an airblast atomizer under elevated ambient pressures, J. Propuls. Power. 26 (2010) 1170–1183, https://doi.org/10.2514/1.47833.
[15] Q.F. Fu, L.J. Yang, Visualization studies of the spray from swirl injectors under elevated ambient pressure, Aerosp. Sci. Technol. 47 (2015) 154–163, https://doi.org/10.1016/j.ast.2015.09.027.
[16] S. Moon, E. Abo-Serie, C. Bae, Air flow and pressure inside a pressure-swirl spray and their effects on spray development, Exp. Therm. Fluid Sci. 33 (2009) 222–231, https://doi.org/10.1016/j.expthermflusci.2008.08.005.
[17] A. Dinc, Optimization of turboprop ESFC and NOx emissions for UAV sizing, Aircr. Eng. Aerosp. Technol. 89 (2017) 375–383, https://doi.org/10.1108/AEAT-12-2015-0248.
[18] S.D. Pack, J.A. Ryon, G.A. Zink, D.D. Dvorak, J.L. Goeke, Spray Diagnostics of a Low NOx Air Blast Atomizer for NASA ERA N + 2 Program united technologies aerospace systems engine components division, in: ILASS Am. 25th Annu. Conf. Liq. At. Spray Syst., 2013.
[19] X. Chen, V. Yang, Effect of ambient pressure on liquid swirl injector flow dynamics, Phys. Fluids. 26 (2014), https://doi.org/10.1063/1.4899261.
[20] H. Hu, T. Saga, T. Kobayashi, N. Taniguchi, A study on a lobed jet mixing flow by using stereoscopic particle image velocimetry technique, Phys. Fluids. 13 (2001) 3425, https://doi.org/10.1063/1.1409537.
[21] H. Hu, T. Saga, T. Kobayashi, K. Okamoto, N. Taniguchi, Evaluation of the cross correlation method by using PIV standard images, J. Vis. 11 (1) (1998) 87–94, https://doi.org/10.1007/BF03182477.
[22] J. Westerweel, Fundamentals of digital particle image velocimetry, Meas. Sci. Technol. 8 (1997) 1379, https://doi.org/10.1088/0957-0233/8/12/002.
[23] L. Gao, Y. Liu, W. Zhou, H. Hu, An experimental study on the aerodynamic performance degradation of a wind turbine blade model induced by ice accretion process, Renew. Energy. 133 (2019) 663–675, https://doi.org/10.1016/J.RENENE.2018.10.032.
[24] Z. Wu, L. Wang, J.A. Badra, W.L. Roberts, T. Fang, GDI fuel sprays of light naphtha, PRF95 and gasoline using a piezoelectric injector under different ambient pressures, Fuel 223 (2018) 294–311, https://doi.org/10.1016/j.fuel.2018.03.009.
[25] S.D. Sovani, E. Chou, P.E. Sojka, J.P. Gore, W.A. Eckerle, J.D. Crofts, High pressure effervescent atomization: effect of ambient pressure on spray cone angle, Fuel 80 (2001) 427–435, https://doi.org/10.1016/S0016-2361(00)00105-8.
[26] X.F. Wang, A.H. Lefebvre, Influence of ambient air pressure on pressure-swirl atomizer spray characteristics, Proc. ASME Turbo Expo (1987), https://doi.org/10.1115/2001-GT-0043.
[27] J. Jedelsky, M. Jicha, J. Slama, J. Otahal, Development of an effervescent atomizer for industrial burners, Energy Fuels 23 (2009) 6121–6130, https://doi.org/10.1021/ef900670g.
[28] J. Jedelsky, M. Maly, N. Pinto del Corral, G. Wigley, L. Janackova, M. Jicha, Air–liquid interactions in a pressure-swirl spray, Int. J. Heat Mass Transf. 121 (2018) 788–804, https://doi.org/10.1016/j.ijheatmasstransfer.2018.01.003.
[29] D. Butcher, A. Spencer, Cross-correlation of pOd spatial modes for the separation of stochastic turbulence and coherent structures, Fluids. 4 (2019), https://doi.org/10.3390/fluids4030134.
[30] X. Fan, G. Xu, C. Liu, C. Zhang, J. Wang, Y. Lin, Experimental investigations of the flow field structure and interactions between sectors of a double-swirl low-emission combustor: effects of main stage swirl intensity and venturi angle, J. Therm. Sci. 29 (2020) 813–819, https://doi.org/10.1007/s11630-020-1228-z.
[31] K. Rajamanickam, S. Basu, On the dynamics of vortex–droplet interactions, dispersion and breakup in a coaxial swirling flow, J. Fluid Mech. 827 (2017) 572–613, https://doi.org/10.1017/jfm.2017.495.
[32] C.T. Crowe, J.D. Schwarzkopf, M. Sommerfeld, T. Yutaka, Multiphase Flows with Droplets and Particles, second ed., CRC Press, Boca Raton, 2011. https://doi.org/10.1201/b11103.
[33] C.E. Brennen, C.E. Brennen, Fundamentals of Multiphase Flow, Cambridge University Press, 2005.
[34] W.R.A. Goossens, Review of the empirical correlations for the drag coefficient of rigid spheres, Powder Technol. 352 (2019) 350–359, https://doi.org/10.1016/j.powtec.2019.04.075.
[35] T.W. Lee, J.E. Park, Determination of the drop size during air-blast atomization, J. Fluids Eng. Trans. ASME. 141 (2019) 1–6, https://doi.org/10.1115/1.4043592.
[36] M. Zhang, M. Xu, D.L.S. Hung, Simultaneous two-phase flow measurement of spray mixing process by means of high-speed two-color PIV, Meas. Sci. Technol. 25 (2014), https://doi.org/10.1088/0957-0233/25/9/095204.